Global Change Biology (2007) **13,** 2110–2127, doi: 10.1111/j.1365-2486.2007.01432.x

Photosynthesis drives anomalies in net carbon-exchange of pine forests at different latitudes

S. LUYSSAERT*†, I. A. JANSSENS*, M. SULKAVA‡, D. PAPALE§, A. J. DOLMAN¶, M. REICHSTEIN‖, J. HOLLMÉN‡, J. G. MARTIN†, T. SUNI**, T. VESALA**, D. LOUSTAU††, B. E. LAW† and E. J. MOORS‡‡

*Department of Biology, University of Antwerp, Universiteitsplein 1, 2610 Wilrijk, Belgium, †College of Forestry, Oregon State University, Corvallis, OR 97331-5752, USA, ‡Laboratory of Computer and Information Science, Helsinki University of Technology, PO Box 5400, 02015 TKK, Finland, §Department of Forest Science and Environment, University of Tuscia, 01100 Viterbo, Italy, ¶Department of Hydrology and Geo-environmental Science, Vrije Universiteit Amsterdam, 1081 HV Amsterdam, The Netherlands, ‖Max Planck Institute for Biogeochemistry, PO Box 100164, 07701 Jena, Germany, **Department of Physical Sciences, University of Helsinki, PO Box 64, 00014 Helsinki, Finland, ††INRA, UR1263 EPHYSE 33883, Villenave d'Ornon, France, ‡‡Alterra, PO Box 47, 6700 AA Wageningen, The Netherlands

Abstract

The growth rate of atmospheric CO_2 exhibits large temporal variation that is largely determined by year-to-year fluctuations in land–atmosphere CO_2 fluxes. This land–atmosphere CO_2-flux is driven by large-scale biomass burning and variation in net ecosystem exchange (NEE). Between- and within years, NEE varies due to fluctuations in climate. Studies on climatic influences on inter- and intra-annual variability in gross photosynthesis (GPP) and net carbon uptake in terrestrial ecosystems have shown conflicting results. These conflicts are in part related to differences in methodology and in part to the limited duration of some studies. Here, we introduce an observation-driven methodology that provides insight into the dependence of anomalies in CO_2 fluxes on climatic conditions. The methodology was applied on fluxes from a boreal and two temperate pine forests. Annual anomalies in NEE were dominated by anomalies in GPP, which in turn were correlated with incident radiation and vapor pressure deficit (VPD). At all three sites positive anomalies in NEE (a reduced uptake or a stronger source than the daily sites specific long-term average) were observed on summer days characterized by low incident radiation, low VPD and high precipitation. Negative anomalies in NEE occurred mainly on summer days characterized by blue skies and mild temperatures. Our study clearly highlighted the need to use weather patterns rather than single climatic variables to understand anomalous CO_2 fluxes. Temperature generally showed little direct effect on anomalies in NEE but became important when the mean daily air temperature exceeded 23 °C. On such days GPP decreased likely because VPD exceeded 2.0 kPa, inhibiting photosynthetic uptake. However, while GPP decreased, the high temperature stimulated respiration, resulting in positive anomalies in NEE. Climatic extremes in summer were more frequent and severe in the South than in the North, and had larger effects in the South because the criteria to inhibit photosynthesis are more often met.

Keywords: Bowen ratio, gross primary production, incident radiation, net ecosystem production, precipitation, respiration, temperature, vapor pressure deficit

Received 10 July 2006; revised version received 27 April 2007 and accepted 3 May 2007

Introduction

The growth rate of atmospheric carbon dioxide (CO_2) varies annually and most of this variability has been attributed to CO_2-fluxes between terrestrial ecosystems and the atmosphere (Bousquet *et al*., 2000). Biomass

Correspondence: S. Luyssaert, Department of Biology, University of Antwerp, Universiteitsplein 1, 2610 Wilrijk, Belgium, e-mail: Sebastiaan.Luyssaert@ua.ac.be

© 2007 The Authors
Journal compilation © 2007 Blackwell Publishing Ltd

burning (van der Werf *et al*., 2004) and climatic variability (Dai & Fung, 1993; Kindermann *et al*., 1996; Braswell *et al*., 1997; Tian *et al*., 1998; Gerard *et al*., 1999; Randerson *et al*., 1999) influence CO_2-fluxes and thus the growth rate of atmospheric CO_2. However, this top–down information, mainly derived from inverse and global modeling, provides relatively little insight into the mechanisms driving the relationships between climatic variability and terrestrial ecosystem processes that influence net ecosystem exchange (NEE, the small net difference of photosynthetic carbon uptake and respiration by autotrophs and heterotrophs).

Although our understanding of carbon cycling in terrestrial ecosystems improved considerably since the development of the eddy covariance technique (Baldocchi, 2003), conflicting results have been reported regarding the relationships between climatic drivers and the intra-annual variability in NEE. Several studies related the variability in NEE to the variability in mean monthly temperature in spring time, summer or fall (Goulden *et al*., 1998; Black *et al*., 2000; Monson *et al*., 2002; Hollinger *et al*., 2004), monthly radiation (Barford *et al*., 2001; Aubinet *et al*., 2002), monthly vapor pressure deficit (VPD) (Aubinet *et al*., 2002), summer drought (Goulden *et al*., 1996), snow depth in winter (Goulden *et al*., 1996), leaf area index (Aubinet *et al*., 2002; Barr *et al*., 2004) and canopy duration (Barr *et al*., 2007). The apparently conflicting results may at least partly be caused by the low temporal resolution used in some analyses. Monthly or seasonal relationships between climatic drivers and NEE might be spurious because weather and NEE vary on a day-to-day basis and longer time periods may include offsetting positive and negative anomalies. In addition, simple relations between CO_2-fluxes and single climatic variables are not particularly helpful and do not represent the more complex interactions of multiple climatic factors and ecosystem processes.

The net exchange of CO_2 between terrestrial ecosystems and the atmosphere is determined by the difference between photosynthetic CO_2 uptake and CO_2 release through autotrophic and heterotrophic respiration, which respond differently to climate and other factors (e.g. substrate availability for heterotrophic respiration; Janssens *et al*., 2001; Law *et al*., 2002). Thus, different climatic conditions can result in similar rates of net ecosystem CO_2-exchange. Net ecosystem CO_2-exchange is typically one order of magnitude smaller than the nearly offsetting terms of photosynthesis and respiration (Goulden *et al*., 1996; Valentini *et al*., 2000). Consequently, small changes in photosynthesis and respiration have to be detected in order to explain relatively large changes in NEE. Nevertheless, if climatic variability is causing anomalous NEE fluxes, the relationships between climate and flux anomalies is likely to be revealed by analyzing high-resolution time series covering several years with different climatic conditions.

This study introduces an observation-driven methodology as a first step in understanding the short-term mechanisms underlying anomalies in ecosystem CO_2-fluxes. To this aim, this methodology: (1) identifies and quantifies daily anomalies in NEE, (2) determines whether these are mainly due to anomalous photosynthesis, anomalous respiration or a combination of both and (3) identifies which combinations of climatic conditions coincide with anomalies in NEE that contribute to the intra-annual variability in NEE.

Material and methods

Experimental sites and data collection

We selected three pine sites for demonstrating our methodological approach: Hyytiälä in Finland, Loobos in the Netherlands and Le Bray in France. These sites were selected because each had 10 years of near continuous flux-tower measurements of NEE and climatic observations. A comparative description of the three sites, including general stand characteristics, climatic features and management aspects is given in Table 1. These three sites differed in many aspects including mean annual temperature, precipitation and incident radiation (Fig. 1), but were all dominated by one plant genus (*Pinus* spp.). The Hyytiälä and Le Bray sites were thinned during the observational period.

Mass and energy fluxes were measured with the eddy covariance technique at all three sites. Details of the measurement system are given in Aubinet *et al*. (2000). Data from all three sites underwent the same processing. First, quality control was performed to filter out suspicious measurements (low nocturnal turbulence, spikes) using a set of standardized tools (Papale *et al*., 2006). Then, missing half-hourly averages were filled using harmonized site-specific artificial neural networks (Papale & Valentini, 2003) to provide more complete datasets. The neural network uses site-specific climatic variables to fill data. Each half-hourly value received a flag representing the quality of the data ranging from original observations (flag 1) to relatively uncertain gap-filled data (flag 3). The flag depends on the length of the gap (autocorrelation of fluxes) and the available meteorological data (covariation of fluxes) to fill it (Reichstein *et al*., 2005). When no input data were available for the neural network, data were filled using the Minimum Distance Sampling method (Reichstein *et al*., 2005). For daily means to be included in the analysis, at least 90% of the 48 half-hourly averages had to be original observations (flag 1) or reliably

© 2007 The Authors

Table 1 General description, site characteristics and data availability of the three pine sites

	Hyytiälä	Loobos	Le Bray	Reference
Latitude (N)	61°05′	52°10′	44°40′	Ceulemans *et al*. (2003)
Longitude (E)	24°17′	5°44′	0°05′	Ceulemans *et al*. (2003)
Elevation (m)	170	25	60	Ceulemans *et al*. (2003)
Country	Finland	the Netherlands	France	
Soil	Sandy	Sandy	Sandy	
Tree species	*Pinus sylvestris*	*P. sylvestris*	*P. pinaster*	Ceulemans *et al*. (2003)
Year of planting	1962	1909	1970	Ceulemans *et al*. (2003)
Year(s) of thinning	2002	–	1996, 1999	Vesala *et al*. (2005)
Tree height (m)	12 (na)	15	17 (18) (19)	Ceulemans *et al*. (2003)
Stand density (number ha^{-1})	2500 (1500)	403	618 (523) (423)	
Peak LAI ($m^2 m^{-2}$)	3 (2)	2	4 (4) (3)	Ceulemans *et al*. (2003), Vesala *et al*. (2005)
Climate	Boreal	Temperate	Temperate	
Mean temperature (°C)	3.5	10.3	13.5	This study
Mean incident radiation ($W m^{-2}$)	99	113	147	This study
Mean annual precipitation (mm)	640	800	900	This study
Time series	1996–2005	1996–2005	1996–2005	
Number of days in time series	2463	2923	2574	This study
Flag 1 data in analyses (%)	63.3	65.7	57.3	This study
Flag 2 data in analyses (%)	36.5	34.1	42.6	This study
Flag 3 data in analyses (%)	0.2	0.2	0.1	This study

The values between brackets are values after thinning.
LAI, leaf area index.

gap-filled (flag 2) data. A threshold of 90% was used: (1) to prevent excessive data loss due to short periods of malfunctioning of the eddy covariance system, such as during dew formation and maintenance and (2) to ensure that responses to environmental conditions are not autocorrelated with environmental variables used for the gap filling. Days with <90% reliable values were excluded from the analysis (Table 1).

The gap-filled NEE was separated into gross primary production (GPP) and ecosystem respiration (R_e) following a generic algorithm that derives a short-term temperature sensitivity (E_0) of respiration from reliable night-time eddy covariance observations and applies this to daytime flux data to compute R_e during the day, and ultimately, GPP (Reichstein *et al*., 2005)

$$R_e(t) = R_{ref}\, e^{E_0(1/(T_{ref}-T_0)-(1/T_{soil}(t)-T_0))},$$

where, T_{ref} is 10 °C, R_{ref} is the temperature independent respiration, T_0 is −46.02 °C and $T_{soil}(t)$ is the soil temperature at time t.

Climatic data were used in gap-filling the NEE time series and in calculating the component fluxes. It is conceivable this introduced a spurious correlation between the climatic data and the fluxes that could be detected later on in the study. However, our analysis focuses on the extreme NEE values and gap-filling algorithms usually do not generate extreme values. Furthermore, we tested the quality of the separation procedure by comparing the component fluxes calculated by the generic algorithm with measurements of day- and night-time NEE. Measurements of daytime NEE from 11:00 hours until 15:00 hours were used as a proxy for GPP. Night-time NEE from 0:00 hours until 03:00 hours was used as a proxy for R_e. Night- and daytime NEE were calculated solely on the basis of original observations (flag 1). As will be described below, these mid-day and midnight data responded similarly, in terms of anomalies, as the separated GPP and R_e fluxes calculated with the generic algorithm. Thus, the correlations between the anomalies in the fluxes and those in climate reported below were not artifacts introduced by the separation approach.

The meteorological data underwent quality control and missing half-hourly averages were filled using Minimum Distance Sampling method (Reichstein *et al*., 2005). Following a quality check of the gap-filling, half-hourly averages were averaged or summed, according to the variable, into daily values which were utilized in this study. Three additional climatic variables were used: daily maximum VPD, daily precipitation and daily Bowen ratio. We used maximum VPD because the average VPD is troublesome because the saturation of water vapor pressure is a function of temperature and temperature is not constant during

© 2007 The Authors

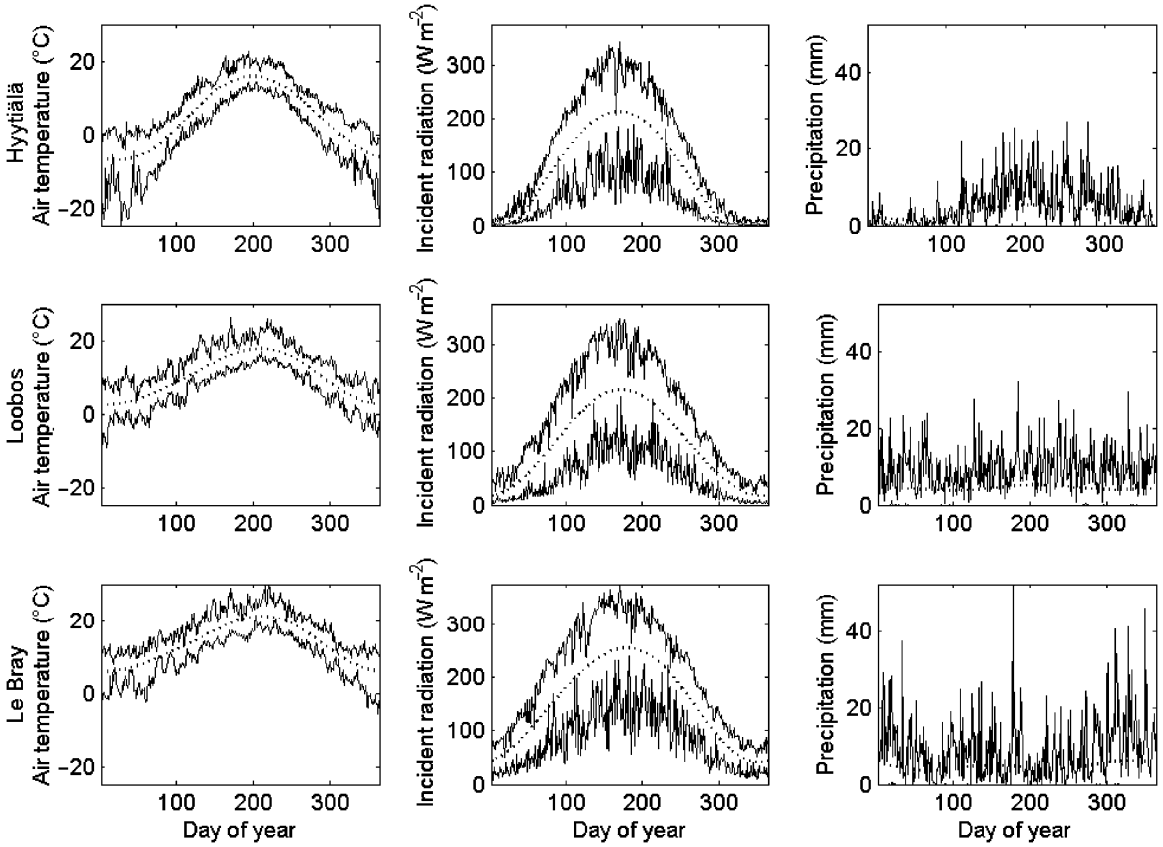

Fig. 1 Seasonal course and variability of the air temperature (°C; left column), incident radiation ($W\,m^{-2}$; middle column) and precipitation (mm; right column) in Hyytiälä (upper panels), Loobos (middle panels) and Le Bray (lower panels). The seasonal course was calculated as the long-term fitted mean (1996–2005) and is given by the dotted line. The observed 10% and 90% percentiles were used as a measure of the observed variability and are given by the full lines.

the day. Therefore, instead of a daily average, the daily maximum observation was used. Precipitation does not occur every day, its time series is thus discrete and therefore hinders processing and interpretation. Suppose, we observe 0 mm of precipitation on a day following 5 days of rain, based on the observed precipitation that day was completely dry. However, the condition of the ecosystem on that single day is likely more similar to a rainy than to a dry day. Therefore, the effect of precipitation (P) was relaxed, henceforth relaxed precipitation, such that $P_{\text{relaxed}}(t) = 0.5(P_{\text{relaxed}}(t-1) + P_{\text{observed}}(t))$. In other words, 50% of the precipitation was assigned to the day that the precipitation occurred (t), 25% to day + 1, 12.5% to day + 2, etc. The relaxed precipitation preserved the observed annual sum and main structure of the observations. In addition, the time series of relaxed precipitation were no longer discrete and could be processed and interpreted as the other climatic variables. Further, relaxed precipitation may be considered as a proxy of the soil water content of the top layer, an important parameter to understand soil respiration. Direct measurements of soil water content were sparsely available for most years. None of the three sites experienced substantial drought stress (see 'Results') and therefore the omission of direct soil water content measurements was thought not to hinder the current analysis. The Bowen ratio is defined as the ratio of sensible to latent heat fluxes and was calculated for all days on which the latent heat was more than $2\,W\,m^{-2}$. The $2\,W\,m^{-2}$ threshold was added to avoid inflation of the ratio during winter in the northernmost site.

Annual time series were subsequently constructed on the basis of daily flux components and climatic conditions. Including 366 days long leap years in the time series would complicate many aspects of the analysis because instead of a 365-day cycle a 1461-day cycle should then be used. Bias is introduced in climate-related trends by giving the calendar date rather than the timing relative to the vernal equinox (Sagarin, 2001). Consequently, all years were aligned such that the vernal equinox occurred on the 80th day (March 21) of the year. Therefore, January 1 from the year before a

© 2007 The Authors
Journal compilation © 2007 Blackwell Publishing Ltd,

leap year was removed from the time series such that every year contained 365 days and all years were aligned on the vernal equinox.

Long-term mean fluxes and flux anomalies

The time series of NEE, GPP and R_e were used to determine both the long-term mean flux and flux anomaly of the component under study. Consequently, the identification of anomalous fluxes depends on how the long-term mean flux rate was determined. The site-specific long-term average was considered the best-available estimator for the expected flux. Thus, longer time series were favored over shorter ones because statistical theory states that the estimated average approaches the true average for an increasing number of observations. Estimating long-term mean fluxes was further constrained by: (1) its seasonal course should to be identical in all years, (2) the seasonal course should be cyclic within a year, i.e. the value for December 31 24:00 hours should equal the value for January 1 0:00 hours, (3) the annual sum of the expected flux should preserve the observed long-term mean annual sum, and (4) the function for the expected NEE should equal the sum of the functions for expected GPP and R_e. Given these constraints, site-specific second-order Fourier functions were fitted to the observations to describe the long-term mean NEE, GPP and R_e. The Fourier function is a sum of sine and cosine functions that is used to describe periodic observations

$$y = a_0 + \sum_{i=1}^{2} a_i \cos(iwx) + b_i \sin(iwx),$$

where, a_0 is a constant (intercept) term in the data and w is the frequency of the observations ($w = 1/365$). When the value of a variable steeply declines at the end of the season to take on almost constant values close to 0 during dormancy and then steeply increases at the start of the next growing season (i.e. GPP and R_g in Hyytiälä), the second-order Fourier function is not able to capture the almost constant values during dormancy. Instead it predicts small positive or negative numbers that are meaningless because neither GPP nor R_g can switch sign. For Hyytiälä, we replaced the predictions for GPP and R_g during dormancy by the mean value of the observations. Initially, the predictions were replaced by the observed value for the period between the days that the predicted values were 0. However, there was a small mismatch between the value at the start and end of dormancy ($=0$) and the observed mean value during that period ($\neq 0$). The length of dormancy was increased and the observed mean value recalculated until the mean observed value during dormancy matched to the predicted value at the start and end of dormancy.

The flux anomalies were then calculated for every day in the time series as the difference between the observed and long-term mean daily flux rate. Every day was thus considered to be anomalous to some extent and the sum of the daily anomalies over the entire observation period equaled 0. When a long-term trend was present in the daily anomalies, we chose not to detrend the anomalies because detrending could remove part of the temporal variability, which is the subject of this study. Consequently, all variability that was not included in the long-term mean flux ended up in the annual anomalies and finally in the interannual variability of the fluxes. This approach cannot be used in developing forests (e.g. young aggrading forests, recently disturbed sites, etc.) because factors other than climate can induce trends. However, it is reasonable to apply this method to developed forests because then the long-term mean is an acceptable estimator of the expected flux response to climate. The Hyytiälä and Le Bray sites were both thinned during the observational period. Thinning raised concerns that the sites experienced variability in fluxes due to the influence of management activities on site-level photosynthesis and respiration. To test this, a Kolmogorov–Smirnov test (H_0: two samples are drawn from the same distribution) was used to compare the anomalies before and after thinning to test whether thinning could have had an influence on the site-level photosynthesis and respiration. In addition, the sensitivity of the anomalies to the length of the time series was quantified using a resampling procedure. Again a second-order Fourier was fitted. However, 1 year of data was left out of the time series. Changes in the expected flux due to a different dataset were reflected in the values of the anomalies. All combinations of the time series with leaving out 1 year of data were made and the number of positive anomalies (determined with the entire time series) that changed into negative anomalies (determined with 1 year less data) and vice versa and the number of changes, which were >20% of the original anomaly were recorded.

Uncertainty of flux anomalies

Uncertainty in NEE was quantified as the random measurement uncertainty, which was calculated as the difference between measurements made under equivalent environmental conditions. This indirect approach of identifying the random uncertainty has been shown to be conservative compared with direct methods which use two independent measurement systems (Richardson *et al*., 2006). We followed Richardson *et al*. (2006) and defined equivalent conditions as: the same time of the day 24 h later, mean half-hourly PPFD within

© 2007 The Authors

$75\,\mu mol\,m^{-2}\,s^{-1}$, air temperature within 3 °C and wind speed within $1\,m\,s^{-1}$. For <10% of the measurements, equivalent environmental conditions were found. Consequently, the time series of the random uncertainties needed to be gap filled to calculate the daily random uncertainty. Gap filling was based on the relationship between NEE and its random uncertainties (Richardson *et al*., 2006). Following, the random uncertainty of daily NEE measurements was calculated as the random uncertainty of all 48 half-hourly measurements within that day whereas the daily random uncertainty of R_e was calculated solely for night-time measurements. Because GPP is calculated as the difference of NEE and R_e, the random uncertainty of GPP was obtained by propagating the random uncertainties of NEE and R_e.

In addition to the artificial neural network approach, the time series of NEE were also gap filled using the Minimum Distance Sampling method (Reichstein *et al*., 2005). For both approaches NEE was separated in R_e and GPP and the differences in fluxes were used as a measure of the uncertainty due to gap filling and flux separation. Finally, the uncertainty of the daily flux anomalies was calculated by propagating the gap filling and flux separation and random uncertainties. However, this value did not include systematic errors due to the instrumentation set-up (Loescher *et al*., 2006).

Annual anomalies and interannual variability

The daily flux anomalies were calculated as the difference between the observed and the expected flux. The annual sum of the daily expected fluxes equaled the long-term mean annual observations for NEE, GPP and R_e. The annual sum of daily anomalies equaled the difference in flux between that year and the long-term mean and was a measure for the annual anomaly. When the annual anomalies were calculated for a calendar year ranging from January 1 until December 31, 10 annual anomalies could be calculated because our time series started on January 1. When the annual anomalies were cumulated over a different annual interval, nine annual anomalies could be calculated with the 10-year time series. The variability between these nine or 10 annual anomalies is the so-called interannual variability. From an ecological point of view, the interannual variability should be calculated from annual intervals beginning at the onset of the growing season, or the start of the water year (e.g. autumn in ecosystems subject to summer drought). However, spring recovery of respiration and photosynthesis and thus the beginning of the growing season is not equivocal across sites in the boreal zone (Suni *et al*., 2003b). Moreover, the starting date of the growing season or water year differs among ecosystems, regions and even from year to year. Hence, there is no well-defined day of the year to start computing the annual anomalies and interannual variability in NEE. Because in our analysis the annual anomalies and interannual variability depend strongly on the chosen starting day, we introduced the annual anomalies as a continuous measure and calculated it for every possible annual interval within the time series ($n = 3286$). Subsequently, the interannual variability was calculated for every day of the year, i.e. the interannual variability between years that start on January 1, the interannual variability between years that start on January 2 and so on ($n = 365$). Consequently, a population of auto-correlated interannual variabilities in NEE was obtained for each site.

Seasonal relationships between fluxes and climatic conditions

Following micrometeorological sign conventions a positive anomaly in NEE represents lower than expected CO_2 uptake or higher than expected CO_2 release from the ecosystem to the atmosphere. The seasonal dependency of the relationships between anomalies in NEE and the coinciding climatic conditions (i.e. observed air temperature, observed incident radiation, observed maximum VPD, relaxed precipitation and Bowen ratio) were quantified by means of stepwise linear regression models. Observations of the climatic conditions from similar 60-day intervals across years were pooled and used to fit a multiple regression model to predict the anomalies in NEE. For each possible 60-day interval ($n = 365$), a separate model was fitted and as such the seasonal course of the regression coefficients was obtained. The observations of the climatic conditions were normalized to allow for the comparison of the different regression coefficients. However, some of the climatic conditions are correlated and therefore the regression coefficients and especially sudden changes should be interpreted with care.

Determinants of flux anomalies

The Self-Organizing Map (SOM) is a well-established artificial neural network for the visualization of high-dimensional data (Kohonen, 2001; Oja *et al*., 2003). We used SOMs to visualize all relationships between anomalies in NEE, anomalies in GPP, anomalies in R_e, observed air temperature, observed incident radiation, observed maximum VPD, relaxed precipitation and Bowen ratio on a daily basis. The component planes of the SOMs of the three sites were plotted in the same figure, to reveal similarities and differences among sites.

© 2007 The Authors

In this study, the SOM was used to sort days on a two-dimensional grid. Each day in the time-series received a single location on the two-dimensional grid and similar days in terms of flux anomalies and climatic conditions received locations near each other on the grid. Consequently, dissimilar days were positioned on different ends of the grid. The *X*- and *Y*-axis of the grid resemble the coordinate system on topographic maps, which justifies the use of the word 'map.' The training algorithm accounted for the flux anomalies and climatic conditions and therefore each location on the grid has a value for each accounted variable. Further elaborating the topographic analogy, the component planes resemble different information layers of the same map. In Fig. 2 each layer has been plotted on the same underlying grid, these plots are called component planes. Different component planes share the same underlying grid and, therefore, an individual day has the same location on each component plane. The *Z*-axis (as given by the colors in the SOM) shows the value of the variable within an information layer. In our case, the *Z*-axis thus contained the values for the flux anomalies and climatic conditions for that grid cell. Technically speaking, the SOM projects complex, nonlinear statistical relationships between high-dimensional data into simple geometric relationships on a regular two-dimensional grid (Kohonen, 2001). These characteristics make the SOM an attractive alternative for some conventional statistical techniques. Technical details of the SOM are expounded in Appendix A.

A clear advantage of the use of a SOM above the use of more conventional visualization tools, i.e. scatter plots is the ability of the SOM to summarize all connections between the flux anomalies and observed climatic conditions in a single figure. As such, the SOM provided a framework for further analysis. Some of

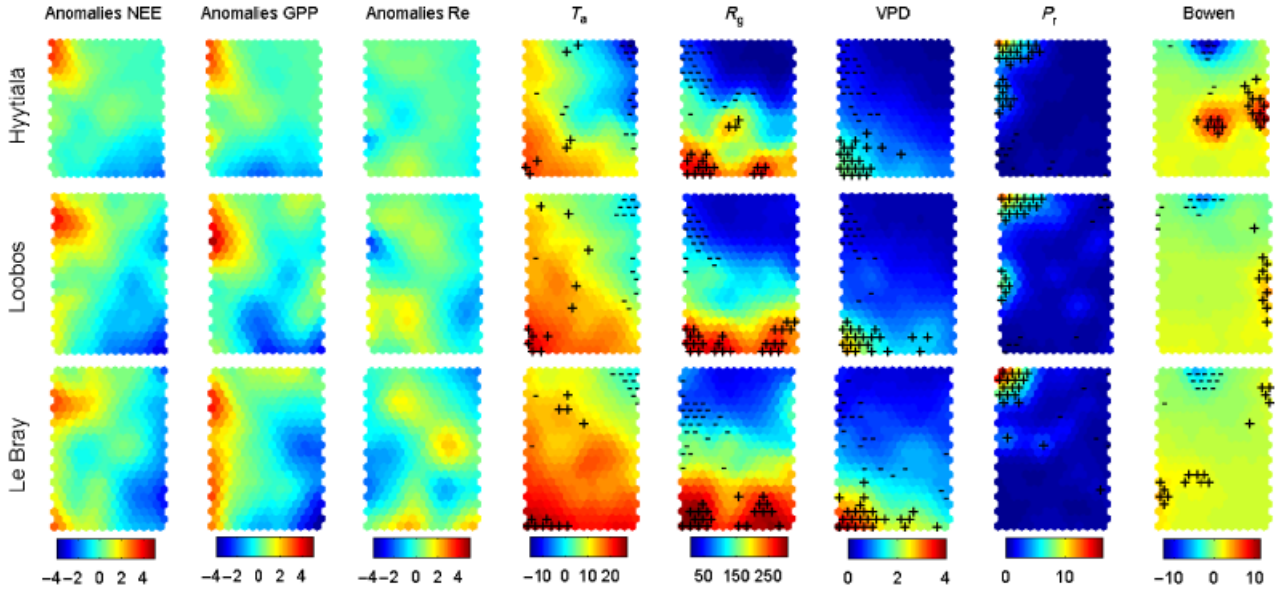

Fig. 2 Component planes for the anomalies in NEE (column 1), GPP (column 2) and R_e (column 3; all in $\mu mol\,CO_2\,m^{-2}\,s^{-1}$) and the corresponding air temperature (T_a, °C; column 4), incident radiation (R_g, $W\,m^{-2}$; column 5), maximal vapor pressure deficit (VPD, kPa; column 6), relaxed precipitation (P_r, mm; column 7) and the Bowen ratio (Bowen, dimensionless; column 8) for Hyytiälä (upper panels), Loobos (middle panels) and Le Bray (lower panels). For the fluxes, positive anomalies indicate more release or less uptake (higher NEE, lower GPP or higher R_e). Negative anomalies indicate more uptake or less release (lower NEE, higher GPP or lower R_e). For each site, each day in the time series received a single location on the two-dimensional grid and similar days in terms of flux anomalies and climatic conditions received locations within the same grid cell or near each other on the grid. Consequently, dissimilar days were positioned on different ends of the grid. The *X*- and *Y*-axis of the grid resemble the coordinate system on topographic maps. The algorithm accounted for the flux anomalies and climatic conditions and therefore each location on the grid has a value for each accounted variable. In our case, the *Z*-axis thus contained the mean values for the flux anomalies and climatic conditions for that grid cell. Further elaborating the topographic analogy, the component planes resemble different information layers of the same map. Each layer has been plotted on the same underlying grid, these plots are called component planes. Different component planes share the same underlying grid and, therefore, an individual day has the same location on each component plane. In each component plane the *Z*-axis (given by the colors) represents a single variable describing the flux anomalies or climatic conditions. Combining the values of all component planes for a given location and site describes the flux anomalies and associated climatic conditions for the days that were allocated to that location. The + and − indicate days on which an extreme high or low anomaly (10% percentile) in the climatic variable was observed. NEE, net ecosystem exchange; GPP, gross photosynthesis; R_e, ecosystem respiration.

© 2007 The Authors
Journal compilation © 2007 Blackwell Publishing Ltd,

the most apparent relationships in the data that were identified by the SOM, are further analyzed with traditional tools such as linear correlation (H_0: no correlation) and cross tabulation (H_0: columns and rows are independent).

Results

Separation of NEE in component fluxes

Because daytime R_e was calculated by means of an algorithm (Reichstein *et al.*, 2005) and GPP was estimated as the difference of daytime R_e and measured NEE, all variability that is not included in the algorithm for calculating R_e ends up in the estimate of GPP. The component fluxes estimated by the generic algorithm were therefore compared with measurements from day- and night-time NEE. The daytime NEE was correlated with calculated daytime GPP and night-time NEE was correlated to the calculated night-time R_e at all three sites (Fig. 3). This shows that the variability in the calculated GPP is due to the variability in photosynthesis and not due to a poor algorithm for separating the component fluxes (see also Reichstein *et al.*, 2007). Furthermore, we also analyzed the temporal variability with measured mid-day and midnight NEE rather than the separated GPP and R_e. Given the strong correlations, it was not a surprise that the results of the analysis with day and night-time NEE yielded very similar results (not shown) as the analysis with the calculated GPP and R_e as presented in this study. Hence, we are confident that our reported results reflect ecological processes at the ecosystem level and not just an artifact of the separation algorithm. The use of the estimated component fluxes was preferred above the use of night- and daytime NEE because the latter is not solely GPP but also contains daytime respiration.

Long-term mean fluxes, flux anomalies and uncertainty

The seasonal course of the long-term mean NEE, GPP and R_e exhibits strong seasonality in Hyytiälä with a long period with almost no fluxes (Fig. 4). Also in Loobos a period with almost no fluxes occurred, but this was much shorter than in Hyytiälä. At Le Bray such a period with extremely small fluxes, did not occur. The long-term average NEE indicated that the pine sites in this study were all carbon sinks between 1996 and 2004 (Table 2). On average, the boreal forest in Hyytiälä accumulated $\sim 215\,g\,C\,m^{-2}\,yr^{-1}$. Although the long-term mean NEE in Loobos ($\sim 400\,g\,C\,m^{-2}\,yr^{-1}$) is larger than in Le Bray ($\sim 275\,g\,C\,m^{-2}\,yr^{-1}$), both the long-term mean photosynthesis and respiration flux are larger in Le Bray than in Loobos (Table 2). The lack of replication within the flux-tower network does, however, not permit the attribution of these differences to tree species or climate.

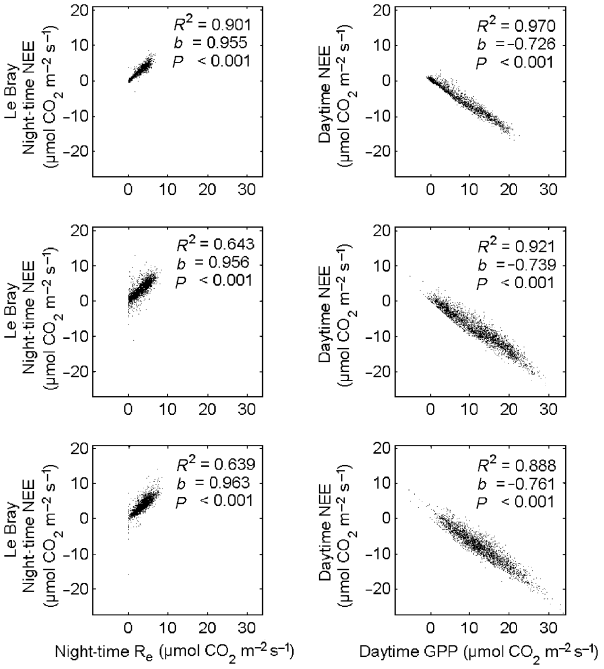

Fig. 3 Relationships between night-time NEE and R_e (left column, $\mu mol\,CO_2\,m^{-2}\,s^{-1}$) and daytime NEE and GPP (right column, $\mu mol\,CO_2\,m^{-2}\,s^{-1}$) in Hyytiälä (upper panels), Loobos (middle panels) and Le Bray (lower panels). NEE, net ecosystem exchange; GPP, gross photosynthesis; R_e, ecosystem respiration.

The gap filling approach was reported to not introduce a bias in the flux anomalies (Moffat *et al.*, 2007). Also, the flux anomalies were generally much larger than their uncertainty (Fig. 5) and therefore considered to be the result of ecological processes instead of random noise due to measurement uncertainty, gap filling and flux separation. Further, we tested the sensitivity of the anomalies to the use of different data subsets (see 'Materials and methods') to describe the long-term mean flux and its uncertainty (Table 2). When different subsets were used for the long-term mean flux, 1.6–2.4% of the negative anomalies became positive anomalies or vice versa. In addition, 73–85% of the resulting changes in the anomalies were smaller than 20% of the original value. Because most of the absolute changes were small, changes in sign mainly occurred for anomalies with a value close to 0. Also when the absolute value of the anomaly changed more than 20% of the original value, the original value was in general very low (data not shown). Consequently, we were confident that the time series were long enough to obtain a robust estimate of the expected seasonal course of NEE, GPP and R_e.

For Hyytiälä, the Kolmogorov–Smirnov test indicated the absence of a noticeable effect of the thinning in 2002

© 2007 The Authors

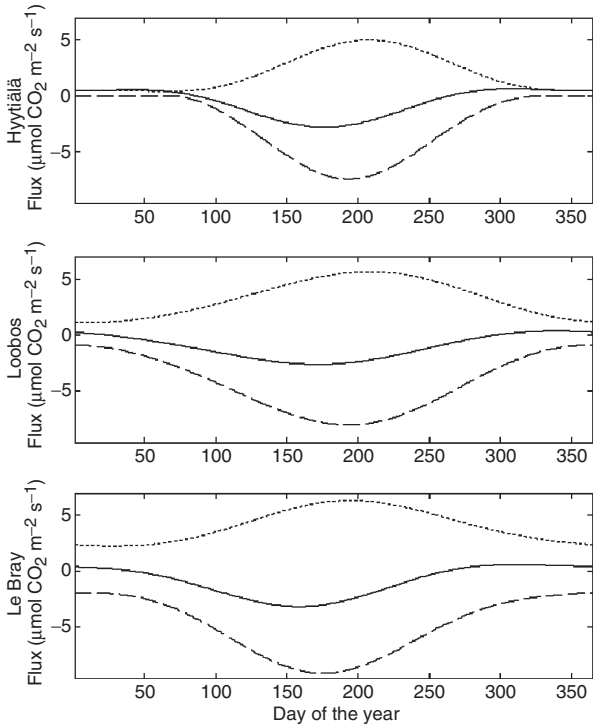

Fig. 4 Seasonal course of the long-term mean NEE, GPP and R_e ($\mu mol\,CO_2\,m^{-2}\,s^{-1}$) in Hyytiälä (upper panel), Loobos (middle panel) and Le Bray (lower panel). The long-term mean was determined by fitting second order Fourier functions to the 10 years time series. The dashed line represents GPP, the dotted line R_e and the full line NEE. NEE, net ecosystem exchange; GPP, gross photosynthesis; R_e, ecosystem respiration.

on the fluxes ($P > 0.05$ for all three fluxes) as was previously documented in detail (Vesala *et al.*, 2005). The effect of the 1996 thinning in Le Bray could not be tested because there were no prethinning data available. However, the distributions of the flux anomalies before and after the thinning in 1999 were different in Le Bray. Consequently, we could not ascertain that the flux anomalies in Le Bray were solely due to climatic variability, at least part of the flux anomalies might be caused by the thinning. Nevertheless, similar relationships between climatic conditions and flux anomalies across all three sites support the case that the flux anomalies were mainly due to the climatic variability.

Annual anomalies and interannual variability

We accounted for the uncertainty in the start of the growing season or water-year by calculating the annual anomalies and their interannual variability for annual intervals starting on different dates. The annual anomalies strongly depended on the starting date of the 365-day period for which they were calculated (Fig. 6). For example, when the considered period began on January 1 and ended on December 31, the three pine forests were C-sinks. When the analyzed period ranged from October 1 to September 30, the forest in Le Bray became C-neutral during the 2001 growing season. Because of the variability in the annual anomalies, also the interannual variability depended on the starting date. We computed the interannual variability for every possible starting date. Owing to the uncertainty in the start of the growing season or water-year, the interannual variability should not be characterized by a single value as is typically done in other studies on this topic. In contrast, interannual variability should be presented as a distribution of possible values (Fig. 4). For the boreal site, the interannual variability calculated as the standard deviation between nine consecutive 365-day periods, can be as low as $\pm 20\,g\,C\,m^{-2}\,yr^{-1}$ (=9% of long-term mean annual sum) and as high as $\pm 52\,g\,C\,m^{-2}\,yr^{-1}$ (=24% of long-term mean annual sum), depending on the starting date. Considerable differences in interannual variability were also observed for the temperate forests (Fig. 6).

Although the dependency between the starting date and annual anomalies and interannual variability seems trivial, it has far reaching consequences. For example, mean annual temperature explained 80% of the interannual variability in NEE in Loobos when the annual interval started on January 1. For an annual interval starting on October 1, mean annual temperature explained <15% of the interannual variability in NEE. Consequently, this kind of time-dependent relationships is unlikely to contribute to the understanding of the causes of interannual variability in NEE. Therefore, we believe that the drivers of interannual variability should be sought within a year instead of between years.

Table 2 Annual sums and 95% confidence intervals of long-term mean NEE, GPP and R_e for the three pine sites ($g\,C\,m^{-2}\,yr^{-1}$) determined by fitting second order Fourier functions to the 10-years time series

Flux		Hyytiälä	Loobos	Le Bray
GPP	Annual sum	-953 ± 16	-1576 ± 26	-1713 ± 56
R_e	Annual sum	738 ± 16	1174 ± 32	1437 ± 36
NEE	Annual sum	-215 ± 12	-402 ± 50	-276 ± 48

NEE, net ecosystem exchange; GPP, gross photosynthesis; R_e, ecosystem respiration.

Seasonal relationships between flux anomalies and climatic conditions

In Hyytiälä substantial positive and negative flux anomalies occur from April through October (Fig. 7). In Loobos and Le Bray substantial anomalies occurred year

© 2007 The Authors

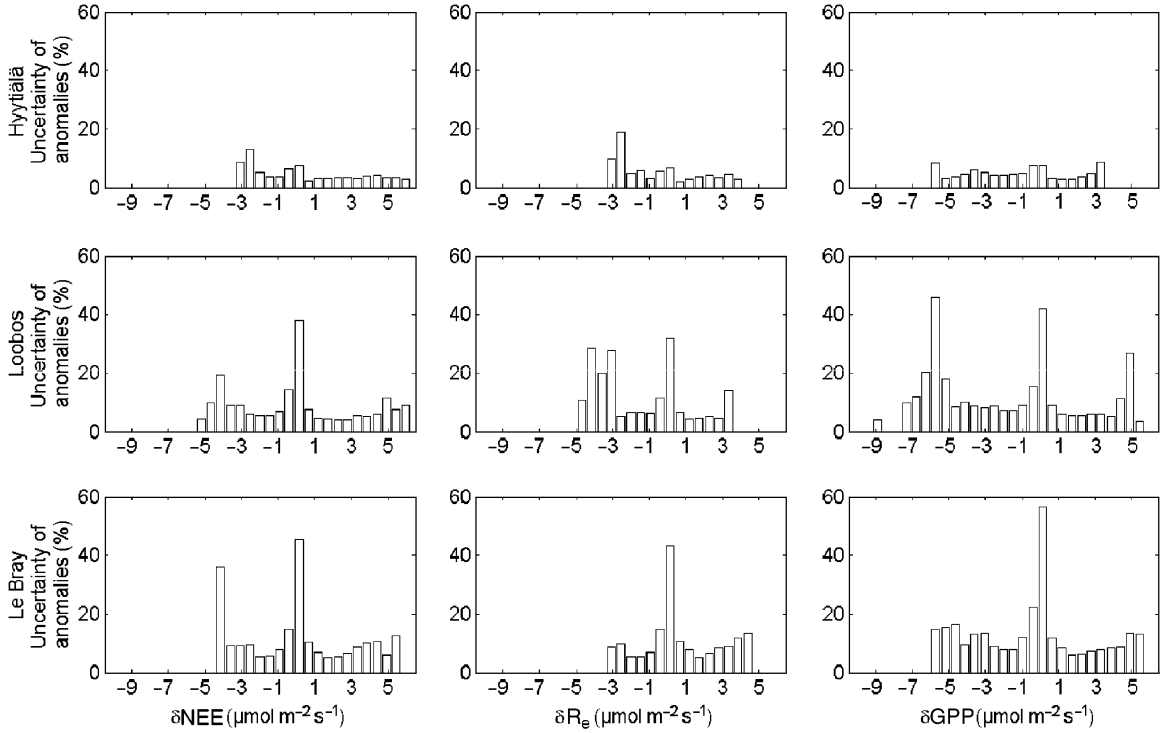

Fig. 5 Flux anomalies of NEE, R_e and GPP and the uncertainty (95% confidence intervals) due to random measurement errors, gap filling and flux separation ($\mu mol\, CO_2\, m^{-2}\, s^{-1}$) in Hyytiälä (upper panel), Loobos (middle panel) and Le Bray (lower panel). NEE, net ecosystem exchange; GPP, gross photosynthesis; R_e, ecosystem respiration.

round, however, some months were more important for positive – and other months for negative flux anomalies.

The relationship between the anomalies in NEE and the climatic conditions were analyzed by means of multiple-regression models. In general, the same relationships between flux anomalies and climatic conditions were found on the different sites, as indicated by the magnitude and sign of the regression coefficients (Fig. 8). Throughout the year and for all three sites, incident radiation was among the most powerful predictors of the anomalies in NEE (Fig. 8); distinct higher radiation was observed during negative NEE anomalies (data not shown). For all three sites, anomalies in NEE were seemingly indifferent to precipitation and the quality of the model was low ($R^2 < 0.4$) in winter. However, timing and length of winter differed between sites.

The predictive power of air temperature, VPD and Bowen ratio showed seasonal and local variability (Fig. 8). In Hyytiälä, high temperatures during early spring were related to higher CO_2 uptake and thus more negative NEE and subsequently a negative regression coefficient. During summer, in contrast, high temperatures coincided with lower net positive CO_2 uptake and thus positive anomalies and subsequently a positive regression coefficient. In contrast to the boreal site in Hyytiälä, anomalies in NEE were almost unrelated to the air temperature during summer in Loobos and Le Bray. In Le Bray, anomalies in NEE were related to VPD during early summer. However, during the same period, no relationship between VPD and flux anomalies was found in Hyytiälä and Loobos. On all three sites, a negative relationship between VPD and NEE anomalies was apparent during autumn although this might be over interpretation of a spurious relationship. The predictive power and the sign of the relationship between NEE anomalies and the Bowen ratio varied during the season and differed between sites. Thus, air temperature, VPD and Bowen ratio were found to have either a positive or negative effect on the anomalies in NEE depending on the time of the year and the site. Consequently, anomalies in NEE were not determined by a single climatic factor but more likely an ensemble of specific conditions is needed to obtain flux anomalies. In the following paragraph, we describe the conditions that coincided with strong negative and positive flux anomalies.

Determinants of flux anomalies

On the NEE planes in Fig. 2, days on which positive anomalies in NEE were observed were colored yellow,

© 2007 The Authors

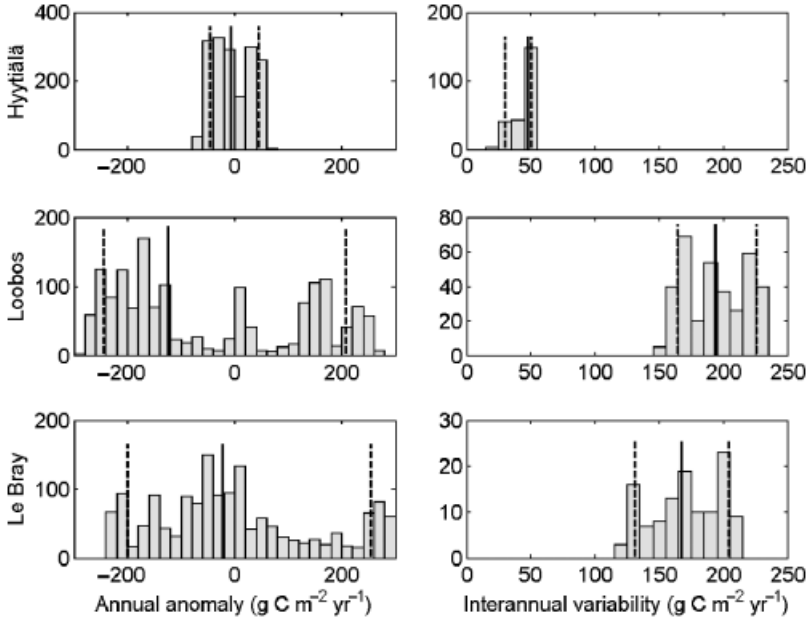

Fig. 6 Distribution of annual anomalies ($g C m^{-2} yr^{-1}$) and interannual variability ($g C m^{-2} yr^{-1}$) calculated for different annual intervals. The full line shows the median whereas the dashed lines indicate the 10th and 90th percentiles. The mean 95% uncertainty interval around the annual anomalies was respectively 8, 12 and 14 $g C m^{-2} yr^{-1}$ for GPP, R_e and NEE in Hyytiälä (Respectively 28, 36 and 42 $g C m^{-2} yr^{-1}$ in Loobos and 22, 23 and 31 $g C m^{-2} yr^{-1}$ in Le Bray). The annual anomaly was calculated over all possible 365-day periods (maximal $n = 3286$) but was not calculated when more than 15% of the daily anomalies were missing within an annual interval. The interannual variability was calculated as the standard deviation between the annual anomalies of at least three and at most nine annual intervals for all possible starting dates (maximal $n = 365$). NEE, net ecosystem exchange; GPP, gross photosynthesis; R_e, ecosystem respiration.

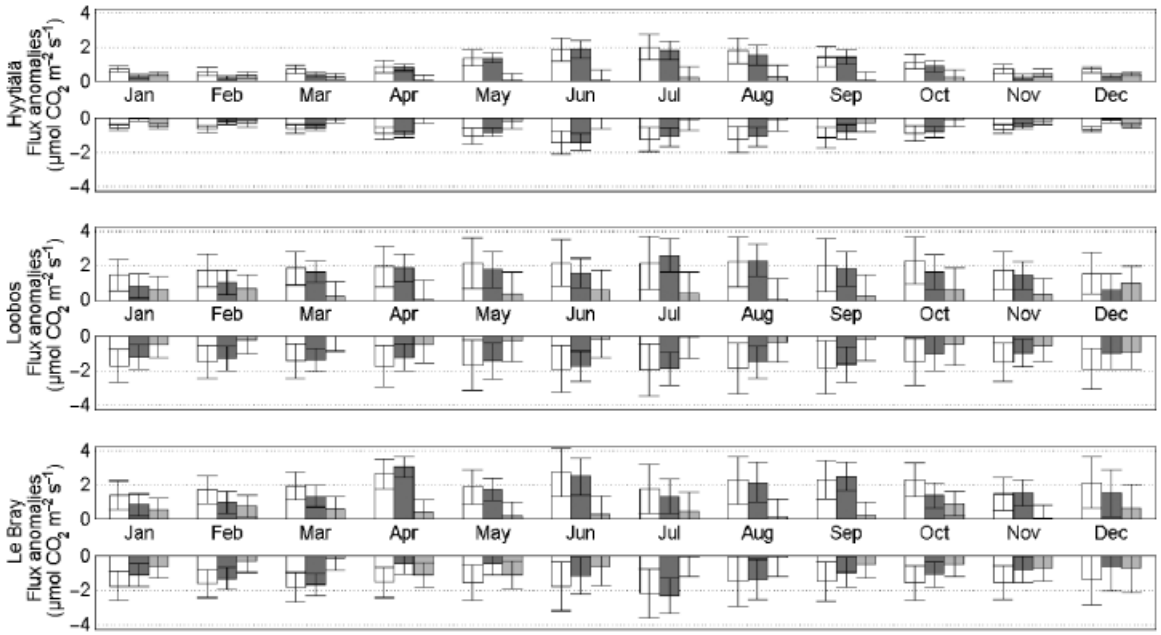

Fig. 7 Seasonal evolution of the daily mean and 95% confidence interval of positive and negative flux-anomalies in NEE (white), GPP (black) and $-R_e$(gray) ($\mu mol CO_2 m^{-2} s^{-1}$) in Hyytiälä (upper panel), Loobos (middle panel) and Le Bray (lower panel). The confidence intervals denote the uncertainty due to random measurement errors, gap filling and flux separation ($\mu mol CO_2 m^{-2} s^{-1}$). NEE, net ecosystem exchange; GPP, gross photosynthesis; R_e, ecosystem respiration.

© 2007 The Authors

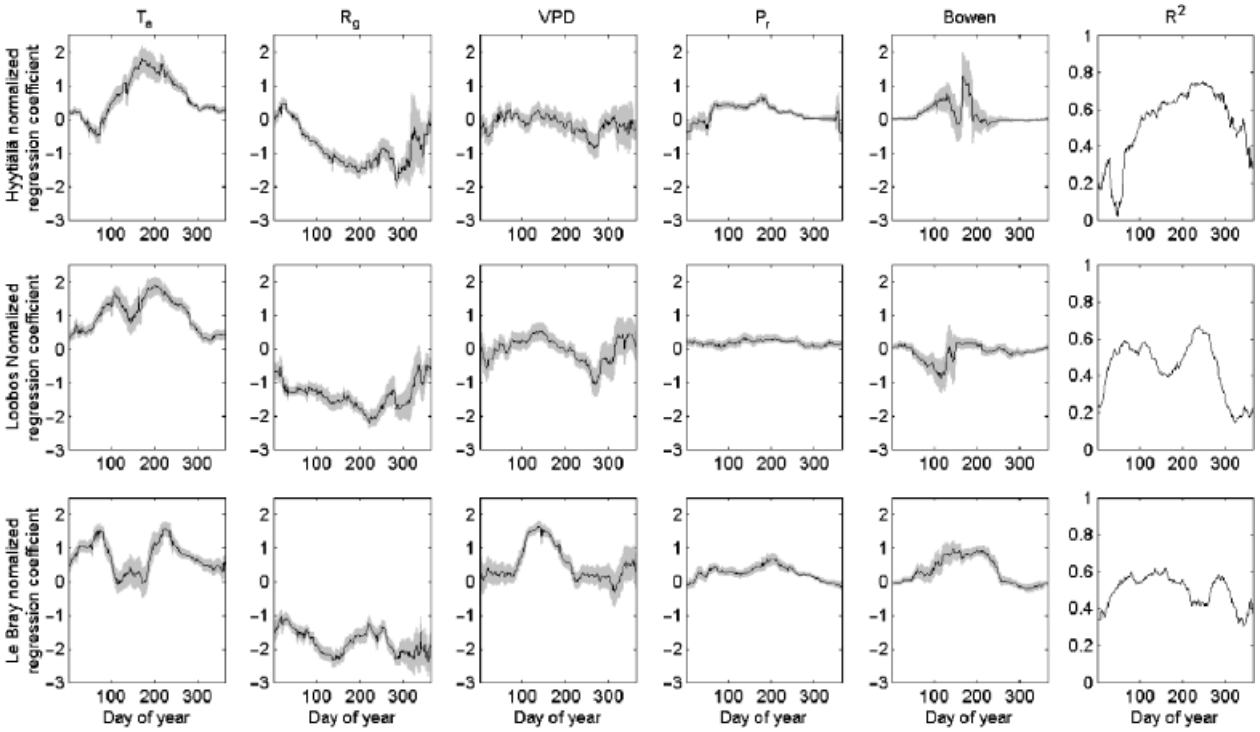

Fig. 8 Seasonal evolution of the normalized regression coefficients and coefficient of determination for a linear stepwise regression model. The model predicts anomalies in net ecosystem exchange from air temperature (T_a), incident radiation (R_g), vapor pressure deficit (VPD), relaxed precipitation (P_r) and Bowen ratio within a 60-day period.

orange or red. When we focus solely on days on which strong positive anomalies were observed (lower CO_2 uptake than expected on that day), the interpretation is limited to the orange and red region on the NEE plane. For the Hyytiälä site, the orange and red region was located in the top-left corner of the NEE plane of the SOM. A single day has the same location on all eight-component planes, hence the top-left corner of the GPP plane shows positive anomalies in GPP (less photosynthetic CO_2 uptake) that coincided with strong positive anomalies in NEE. For all three sites, positive anomalies in NEE (2.5, 2.9 and 1.9 $\mu mol\,CO_2\,m^{-2}\,s^{-1}$ for Hyytiälä, Loobos and Le Bray, respectively) occurred mainly on days with an air temperature between 10 and 20 °C, an incident radiation below 100 $W\,m^{-2}$, a maximal VPD below 0.7 kPa and a Bowen ratio between −5 and 2 (Fig. 2; top-left corner of the different component planes; χ^2-test: $P<0.01$ for all three sites). Typically, relaxed precipitation during these periods of low carbon uptake exceeded 2 mm day^{-1} indicating that these climatic conditions were associated with rain events. These conditions were observed on days with positive anomalies in GPP (χ^2-test: $P<0.01$ for all three sites; 2.4, 2.9 and 1.7 $\mu mol\,CO_2\,m^{-2}\,s^{-1}$ for Hyytiälä, Loobos and Le Bray, respectively) and no clear signal for the anomalies in R_e (χ^2-test: $P>0.18$ for all three sites; 0.1, 0.1 and 0.2 $\mu mol\,CO_2\,m^{-2}\,s^{-1}$ for Hyytiälä, Loobos and Le Bray, respectively). Positive anomalies in GPP are related to photosynthesis that is lower than the long-term mean for the time of the year. As a result the ecosystems behaved as a stronger carbon source than expected. Clearly, air temperature itself did not discriminate between positive and negative anomalies in NEE in Loobos and Le Bray (χ^2-test: $P=0.07$ for Hyytiälä, $P=0.49$ for Loobos and $P=0.96$ for Le Bray).

Anomalously high carbon uptake and low NEE (−0.7, −0.8 and −0.5 $\mu mol\,CO_2\,m^{-2}\,s^{-1}$ for Hyytiälä, Loobos and Le Bray, respectively; Fig. 2 bottom-right corner) occurred when incident radiation exceeded 100 $W\,m^{-2}$, maximal VPD was between 0.7 and 1.3 kPa and Bowen ratio was between 0 and 2 (χ^2-test: $P<0.01$ for all three sites for GPP and NEE). Relaxed precipitation was typically below 2 mm day^{-1}, indicating that these climatic conditions did not prevail on rainy days.

A strong relationship was evident between anomalies in NEE and anomalies in GPP (Fig. 2): for Hyytiälä $r^2=0.74$, for Loobos $r^2=0.60$, and for Le Bray $r^2=0.51$ ($P<0.01$ for all three sites). Anomalies in NEE and anomalies in R_e were weakly correlated on all three sites ($r^2=0.03$ for Hyytiälä, $r^2=0.09$ for Loobos and $r^2=0.02$ for le Bray). The dominance of GPP may be determined by the chosen temporal scale because the

© 2007 The Authors
Journal compilation © 2007 Blackwell Publishing Ltd,

almost instantaneous effects of climate variables on GPP are clearer on a daily basis than the lagged responses of respiration (Ryan & Law, 2005). Nevertheless, accounting for a 1–30-day lag did not alter the contribution of R_e to daily anomalies in NEE (data not shown). Consequently, anomalies in NEE were most often dominated by anomalies in GPP.

Typically, on days that R_e was stimulated (0.3, 0.5 and 0.2 $\mu mol\,CO_2\,m^{-2}\,s^{-1}$ for Hyytiälä, Loobos and Le Bray, respectively), photosynthesis was stimulated as well (−0.6, −0.6 and −0.8 $\mu mol\,CO_2\,m^{-2}\,s^{-1}$ for Hyytiälä, Loobos and Le Bray, respectively). Hence, these days only marginally contributed to the annual anomaly in NEE (−0.3, −0.1 and −0.6 $\mu mol\,CO_2\,m^{-2}\,s^{-1}$ for Hyytiälä, Loobos and Le Bray, respectively). Compensation of increased respiratory fluxes can be clearly seen for almost all positive anomalies in R_e in Fig. 2 (yellow and orange areas on the R_e plane coincide with blue areas on the GPP plane). However, at the southernmost site in Le Bray, R_e was further stimulated (0.4 $\mu mol\,CO_2\,m^{-2}\,s^{-1}$) during hot, clear and very dry periods (χ^2-test: $P = 0.10$). However GPP was in part inhibited during these conditions ($+1.7\,\mu mol\,CO_2\,m^{-2}\,s^{-1}$; χ^2-test: $P = 0.01$; Fig. 2 bottom-left yellow–orange triangle on the R_e plane of Le Bray). Hence, the anomalies in GPP no longer offset the anomalies in R_e. Thus, anomalies in R_e were offset by anomalies in GPP up to a critical threshold of 300 $W\,m^{-2}$ and maximal VPD above 2.0 kPa above which the anomalies in R_e contribute to the anomalies in NEE (2.1 $\mu mol\,CO_2\,m^{-2}\,s^{-1}$).

Averaging daily anomalies over multiple-day periods lowers the temporal resolution and could reveal relationships between ecosystem processes that take longer than 1 day to establish. Averaging the anomalies in NEE and R_e over a 4–5-day period increased the r^2 of the linear relationship between both fluxes from below 0.09 to 0.18 for all three sites. The effect of warm (>15 °C), overcast weather (<150 $W\,m^{-2}$) with a moderate maximal VPD (<1.3 kPa) in Le Bray increased as these weather conditions persisted inducing strong anomalies in R_e (0.8 $\mu mol\,CO_2\,m^{-2}\,s^{-1}$; χ^2-test: $P < 0.01$) that were reflected in the anomalies in NEE (0.3 $\mu mol\,CO_2\,m^{-2}\,s^{-1}$; results based on SOMs for averaged values; not shown). The monthly flux anomalies in R_e correlated with the previous month anomalies in GPP (r^2 ranging from 0.16 to 0.48), confirming that R_e is partly driven by recent photosynthesis.

During drought stress, the sensible heat flux is expected to be high whereas the latent heat flux is expected to be low due to water shortage. This situation would then result in a high Bowen ratio. Apart from spring in Hyytiälä the Bowen ratio was never high and thus never indicated drought stress. In Hyytiälä the sensible heat flux quickly increases during spring because the soil heats up after snowmelt (Launiainen *et al.*, 2005). The soil can heat up by as much as 9 °C on a single day (Suni *et al.*, 2003b). However, at that time in spring, most of the snow has already melted and the latent heat flux is not remarkably high. Although the Bowen ratio is very high during that time of spring, it did not coincide with anomalous fluxes (Fig. 2).

Relationships between daily and annual anomalies

In Loobos, the average daily anomaly in NEE during summer was +2.0 or −1.3 $g\,C\,m^{-2}\,day^{-1}$ for positive and negative anomalies, respectively (Fig. 7), whereas the median annual anomalies in NEE amounted 100 $g\,C\,m^{-2}\,yr^{-1}$ (Fig. 6). In the absence of negative anomalies, on average 50 summer days with a positive anomaly are needed to add up to the average annual anomaly. The magnitude of the daily anomalies was small compared with annual anomalies and therefore many daily anomalies are needed to explain a substantial part of the annual anomalies.

On average, the 120 largest NEE daily anomalies per year explained 70% of the total annual anomaly in NEE in Hyytiälä. Because daily anomalies were small from November to March, these 5 months did not contribute substantially to the annual anomalies (Fig. 7). The contribution of daily anomalies to the total annual anomalies increased from April to July and then decreased towards October and thus the annual anomalies were mainly yielded from late spring to early fall. Throughout the year photosynthesis dominated the anomalies in NEE (Fig. 7). For Loobos and Le Bray, cumulating the 100 largest daily anomalies explained 70% of the total annual anomalies in NEE. In Loobos and Le Bray all months contributed to the annual anomalies, although the contribution of spring and summer months dominated. Consequently, annual anomalies cannot easily be attributed to single isolated anomalies.

Discussion

Determinants of flux anomalies

Compared with other boreal forests, the stand in Hyytiälä, which is located in the south of the boreal zone, is a substantial carbon sink (215 $g\,C\,m^{-2}\,yr^{-1}$). Measured NEE for boreal evergreen coniferous forests in the flux-tower network (excluding Hyytiälä) ranged from a carbon source of 110 $g\,C\,m^{-2}\,yr^{-1}$ on afforested drained peat to a carbon sink of 170 $g\,C\,m^{-2}\,yr^{-1}$ on mineral soil (Law *et al.*, 2002). The two temperate pine forests accumulated on average 275 and 400 $g\,C\,m^{-2}\,yr^{-1}$. These values agree with reported sink-strengths for temperate evergreen coniferous forests within the net-

© 2007 The Authors

work (Law *et al*., 2002; excluding Loobos and Le Bray). In addition, the interannual variability in this study (between 20 and 234 $g C m^{-2} yr^{-1}$) was of the same magnitude as in the few other studies on the subject: $\pm 46 g C m^{-2} yr^{-1}$ in a spruce forest at the Howland site (Hollinger *et al*., 2004), $\pm 35 g C m^{-2} yr^{-1}$ in a hardwood forest at the Harvard site (Goulden *et al*., 1996; Barford *et al*., 2001) and $\pm 92 g C m^{-2} yr^{-1}$ in an aspen forest in Prince Albert National Park, Saskatchewan, Canada (Black *et al*., 2000).

In this study, the interannual variability given by the standard deviation of annual anomalies highly depended on the annual interval that was used. Moreover, the relationships between the interannual variability and the climatic conditions also depended on the interval. Consequently, the annual interval is not the appropriate scale to interpret ecosystem functioning. Annual anomalies are difficult to interpret, and subannual intervals that focus on seasons or smaller intervals are better for relating specific ecological processes to the observed anomalies.

An analysis of monthly flux anomalies in a spruce-hemlock forest showed that above-average summer temperatures were correlated with decreased net carbon uptake (Hollinger *et al*., 2004). However, no significant impact of air temperature was observed in a temperate Douglas fir stand (Aubinet *et al*., 2002). In this Douglas fir stand, the temporal variability in NEE correlated with monthly mean radiation and VPD (Aubinet *et al*., 2002). Our results confirm the correlation between radiation and temporal variability in NEE. However, the correlations between the temporal variability in NEE and the other climatic variables (air temperature, VPD, relaxed precipitation and Bowen ratio) varied within the season and across sites (Fig. 8). The variability across sites is likely caused by the fact that the climatic conditions across sites are very different. For example, spring and fall temperatures in Le Bray are similar to the summer temperatures in Hyytiälä. Thus, when a process is determined by temperature, a similar effect is expected in Le Bray and Hyytiälä but the effect will occur in different seasons. Therefore, the analysis should be based on absolute climatic conditions because similar anomalies (e.g. $+1\,^{\circ}C$) can occur in different seasons. Further, the seasonal variability of the relationships between climatic conditions and anomalies in NEE suggests that the latter were not determined by a single climatic condition but more likely by an ensemble of climatic conditions.

At our three sites, negative anomalies in NEE are in general caused by increased photosynthesis, not by reduced respiration. Averaged over six sites, GPP was reported to dominate the temporal NEE patterns (van Dijk *et al*., 2005). Similarly, the temporal variability of NEE was controlled mostly by the temporal variability in GPP for a 23 and 89 years old pine stand that experiences summer drought (Schwarz *et al*., 2004). On all three sites, respiration was in part driven by recent photosynthates as was previously shown on other sites (Ekblad & Högberg, 2001; Tang *et al*., 2005). Even during episodes of increased R_e, its effect was hardly reflected in the NEE because increases in R_e typically coincided with increases in GPP (except during very hot weather). The majority of the negative anomalies are observed on sunny days that are not very hot i.e. the air temperature is between 10 and 18 °C, the incident radiation is above $100 W m^{-2}$, the maximal VPD is between 0.7 and 1.3 kPa, the Bowen ratio is between 0 and 2, and the relaxed precipitation is <2 mm. Positive anomalies tended to be caused by a decreased photosynthesis at all three sites and are typically observed on rainy days with an air temperature between 10 and 18 °C, a incident radiation below $100 W m^{-2}$, a maximal VPD below 0.7 kPa, a Bowen ratio between from -5 to 2 and relaxed precipitation exceeding 2 mm. Across all three sites, the main sources of intra-annual variability in NEE are radiation and VPD. Positive and negative anomalies occur at the same temperature and therefore, there is only minor impact of temperature on the temporal variability of the fluxes. However, temperature is correlated to other climatic variables and therefore high spring and fall temperatures are most likely to be observed on a clear day. Consequently, the climatic conditions on these days resemble the conditions observed on a day with a negative anomaly in NEE. Hence, above-average spring and fall temperatures are expected to correlate with greater carbon uptake as reported for a spruce-hemlock forest (Hollinger *et al*., 2004).

Although temperature is in general not discriminating between positive and negative anomalies in NEE, it does become important when the mean daily air temperature exceeds 23 °C. On such days the mean incident radiation exceeds $250 W m^{-2}$ but GPP is nonetheless reduced, likely because the maximal VPD typically exceeds 2.0 kPa. Moreover, the high temperature stimulates respiration (the three sites were not drought affected) and as a result positive anomalies in NEE occur. Only on these hot days respiration dominates the flux anomaly in NEE, which is in line with the reported higher increase in R_e than in GPP at higher temperatures (van Dijk *et al*., 2005). At the northern site, extreme climatic conditions in summer rarely meet the criteria to inhibit photosynthesis. Because climatic extremes in summer are more severe in the South than in the North, they have larger effects in the South. Hence, sites in which the mean daily temperature frequently exceeds 23 °C are expected to exhibit positive anomalies in NEE

© 2007 The Authors

during summer. This temperature threshold might differ between plant genera and between climatic zones, and therefore needs not be valid for other ecosystems.

Future climate is predicted to bring more frequent and longer lasting heatwaves (Meehl & Tebaldi, 2004; Schär *et al*., 2004). In such years, our results suggest reduced photosynthesis and net ecosystem CO_2 uptake in pine forests (similar to Ciais *et al*., 2005). Reduced photosynthesis and net ecosystem CO_2 uptake are also expected in years with more frequent and longer lasting periods with low radiation and high precipitation. Only an increase in the number of warm clear days in the absence of water stress would result in photosynthesis and net CO_2 uptake exceeding the current long-term mean fluxes for pine forests.

Relationships between daily and annual anomalies

Spring temperature is reported to be so influential on NEE that it not only affects the daily anomalies, it also determines the entire annual anomaly (Goulden *et al*., 1998; Chen *et al*., 1999; Black *et al*., 2000; Barr *et al*., 2004; Kljun *et al*., 2006). For example, annual anomalies in NEE were reported to correlate to spring temperature in a boreal spruce forest (Goulden *et al*., 1998; Kljun *et al*., 2006) and in several boreal deciduous forest ecosystems (Chen *et al*., 1999; Black *et al*., 2000; Barr *et al*., 2004). Spring temperature is thought to control NEE mainly via the influence of air temperature on the timing of leaf emergence (Chen *et al*., 1999), such that in years with a warm spring, carbon uptake is higher than expected and results in negative annual anomalies in NEE. Our results do not support the idea that spring temperature in itself correlates to the annual anomalies in NEE in the boreal zone. During the spring months April and May, a daily negative anomaly in NEE (indicating higher CO_2 uptake than expected) is on average $-0.63\,g\,C\,m^{-2}\,day^{-1}$ in Hyytiälä (Fig. 7). A daily positive anomaly is on average $+0.70\,g\,C\,m^{-2}\,day^{-1}$ in spring (Fig. 7). Now assume that for every warm spring day an average positive anomaly is replaced by an average negative anomaly. A warm spring day would then affect the annual anomaly by $-1.33\,g\,C\,m^{-2}\,day^{-1}$ (-0.63–$0.70\,g\,C\,m^{-2}\,day^{-1}$). An advancement of spring by 10 days would add on average $-13.3\,g\,C\,m^{-2}$ to the annual anomalies. Recall that the annual anomalies in Hyytiälä ranged between -68 and $+66\,g\,C\,m^{-2}\,yr^{-1}$ (Fig. 6). A similar reasoning holds for flux-anomalies at Loobos and Le Bray. Consequently, a single climatic event which lasts for a couple of days contributes to the annual anomaly but is unlikely to dominate it. Many more anomalous days that contribute to the annual anomaly precede or follow the event. Our results suggest that in order to contribute to the annual anomaly, increased spring temperature needs to cause a long-lasting condition that favors negative anomalies in NEE. In this context, long-lasting means at least 50–100 days. An increased leaf area index due to increased spring temperatures could be such a long-lasting effect that favors negative anomalies in NEE (Barr *et al*., 2004).

Observation-driven methodologies

In contrast to most other analysis of the interannual variability, this study used a daily resolution for the identification and quantification of the anomalies and the analysis of their dependence on ensembles of climatic conditions. Because we studied the same phenomena in similar ecosystems (and even the same forest) as in some of the above-mentioned papers, it is not a surprise that we find similar results. Some differences in response between our work and earlier studies could not be resolved. Although an earlier study of the Hyytiälä reported only weak relationships between climate conditions and temporal variability in NEE (Suni *et al*., 2003a), we found consistent relationships between flux anomalies and climatic variability. The earlier study searched relationships between climatic conditions and flux anomalies averaged over the length of an entire season. A season encompasses several contrasting climatic conditions and consequently underlying relationships are smoothed. The study of Carrara *et al*. (2003) revealed a correlation between the interannual variability and the length of the growing season. The residuals of this relationship correlated with the mean annual temperature. However, length of the growing season is not a climatic variable but likely caused by a suite of climatic conditions. It is therefore difficult to interpret the relationship between the residuals and temperature because spring and fall temperature are likely among the causes of the longer growing season. The methodological approaches of Suni *et al*. (2003a) and Carrara *et al*. (2003) were too different from ours and therefore their results can not easily be related to our analysis.

The chosen resolution partly determines the results irrespective of whether a monthly, weekly or daily resolution has been used. However, the ecosystem does not function on a day-by-day, week-by-week or month-by-month basis. The same climatic conditions can persist for <1 day up to weeks, some climatic conditions are mutually exclusive and past events can strengthen or offset the effect of a current event. In addition, different processes such as photosynthesis and respiration operate on different temporal scales (Bowling *et al*., 2002; Stoy *et al*., 2005). Better understanding of the mechanisms behind interannual variability requires future work to develop methodological approaches that

© 2007 The Authors

study the ecosystem process on their most appropriate resolution and account for delayed interactions.

Conclusion

Owing to the length of the time series (i.e. 10 years), simple correlations between annual flux numbers and annual numbers characterizing climatic conditions were found to be too sensitive to extreme values to be used as the main tool for studying interannual variability. Therefore, the drivers of interannual variability were studied within a year rather than between years. The seasonal variability of the relationships between climatic conditions and anomalies in NEE suggested that the latter were not determined by single climatic conditions but more likely by an ensemble. We studied the relationships between ensembles of climatic conditions and flux anomalies on a daily basis.

The daily flux anomalies showed a clear seasonal pattern in the boreal forest. The contribution of the daily flux anomalies to the annual anomaly increased from spring to summer, reached a maximum in midsummer and decreased during fall to become negligible in wintertime. At the temperate sites, there were no clear seasonal patterns in flux anomalies and nearly every day of the year can potentially contribute to the annual anomaly. Consequently, the annual anomalies were determined in a much shorter time period at the boreal site than at the temperate sites. In any case, single multiple-day events are unlikely to dominate the annual anomaly in NEE unless they induce long-lasting effects.

The annual anomalies in NEE are dominated by GPP in all three studied pine forests. Anomalies in R_e frequently occurred but were typically offset by anomalies in GPP. Owing to increased GPP, a stronger carbon sink than the long-term mean for the time of the year was observed on days with high radiation, high VPD and low relaxed precipitation. The studied pine forests exhibit positive anomalies in NEE, on extreme hot days (reduced GPP and increased R_e) and on days characterized by low radiation, low VPD and high-relaxed precipitation (reduced GPP). Toward the South, extreme hot days with high values for air temperature (i.e. $T_a > 23\,^{\circ}C$), incident radiation and VPD are more frequently observed. Given that on these days pine forest releases more CO_2 to the atmosphere than expected, a reduction in net CO_2 uptake is to be expected in years that more and longer lasting periods with high temperatures occur.

Acknowledgements

Data collection and processing was funded by CarboEurope-IP and preceding projects supported by the European Commission and national funding by the countries of the different participating institutes, the Research Foundation – Flanders (FWO-Vlaanderen) supported S.L. with a postdoctoral fellowship and a research grant. The graduate school of the Department of Computer Science and Engineering at TKK supported M. S. J. H. and M. S. received funding from the Academy of Finland. The Nordic Centre of Excellence NECC and REBECCA supported the Department of Physical Sciences at the University of Helsinki.

References

Aubinet M, Grelle A, Ibrom A *et al*. (2000) Estimates of the annual net carbon and water exchange of forests: the EUROFLUX methodology. *Advances in Ecological Research*, **30**, 113–175.

Aubinet M, Heinesch B, Longdoz B (2002) Estimation of the carbon sequestration by a heterogeneous forest: night flux corrections, heterogeneity of the site and inter-annual variability. *Global Change Biology*, **8**, 1053–1071.

Baldocchi D (2003) Assessing the eddy covariance technique for evaluating carbon dioxide exchange rates of ecosystems: past, present and future. *Global Change Biology*, **9**, 479–492.

Barford CC, Wofsy SC, Goulden ML *et al*. (2001) Factors controlling long- and short-term sequestration of atmospheric CO_2 in a mid-latitude forest. *Science*, **294**, 1688–1691.

Barr AG, Black TA, Hogg EH, Griffis TJ, Morgenstern K, Kljun N, Theede A, Nesic Z (2007) Climatic controls on the carbon and water balances of a boreal aspen forest, 1994–2003. *Global Change Biology*, **13**, 561–576.

Barr AG, Black TA, Hogg EH, Kljun N, Morgenstern K, Nesic Z (2004) Inter-annual variability in the leaf area index of a boreal aspen-hazelnut forest in relation to net ecosystem production. *Agricultural and Forest Meteorology*, **126**, 237–255.

Black TA, Chen WJ, Barr AG *et al*. (2000) Increased carbon sequestration by a boreal deciduous forest in years with a warm spring. *Geophysical Research Letters*, **27**, 1271–1274.

Bousquet P, Peylin P, Ciais P, Le Quere C, Friedlingstein P, Tans PP (2000) Regional changes in carbon dioxide fluxes of land and oceans since 1980. *Science*, **290**, 1342–1346.

Bowling DR, McDowell NG, Bond BJ, Law BE, Ehleringer JR (2002) C-13 content of ecosystem respiration is linked to precipitation and vapor pressure deficit. *Oecologia*, **131**, 113–124.

Braswell BH, Schimel DS, Linder E, Moore B (1997) The response of global terrestrial ecosystems to interannual temperature variability. *Science*, **278**, 870–872.

Carrara A, Kowalski AS, Neirynck J, Janssens IA, Yuste JC, Ceulemans R (2003) Net ecosystem CO_2 exchange of mixed forest in Belgium over 5 years. *Agricultural and Forest Meteorology*, **119**, 209–227.

Ceulemans R, Kowalski A, Berbigier P *et al*. (2003) Coniferous forests (Scots and maritime pine): carbon and water fluxes, balances, ecological and ecophysiological determinants. In: *Fluxes of Carbon Water and Energy of European Forests. Ecological Applications*, Vol. 163 (ed. Valentini R), pp. 71–97. Springer Verlag, Berlin.

Chen WJ, Black TA, Yang PC *et al*. (1999) Effects of climatic variability on the annual carbon sequestration by a boreal aspen forest. *Global Change Biology*, **5**, 41–53.

© 2007 The Authors
Journal compilation © 2007 Blackwell Publishing Ltd,

Ciais P, Reichstein M, Viovy N *et al*. (2005) Europe-wide reduction in primary productivity caused by the heat and drought in 2003. *Nature*, **437**, 529–533.

Dai A, Fung IY (1993) Can climate variability contribute to the missing CO_2 sink. *Global Biogeochemical Cycles*, **7**, 599–609.

Ekblad A, Högberg P (2001) Natural abundance of C-13 in CO_2 respired from forest soils reveals speed of link between tree photosynthesis and root respiration. *Oecologia*, **127**, 305–308.

Gerard JC, Nemry B, Francois LM, Warnant P (1999) The interannual change of atmospheric CO_2: contribution of subtropical ecosystems? *Geophysical Research Letters*, **26**, 243–246.

Goulden ML, Munger JW, Fan SM, Daube BC, Wofsy SC (1996) Exchange of carbon dioxide by a deciduous forest: response to interannual climate variability. *Science*, **271**, 1576–1578.

Goulden ML, Wofsy SC, Harden JW *et al*. (1998) Sensitivity of boreal forest carbon balance to soil thaw. *Science*, **279**, 214–217.

Hollinger DY, Aber J, Dail B *et al*. (2004) Spatial and temporal variability in forest–atmosphere CO_2 exchange. *Global Change Biology*, **10**, 1689–1706.

Janssens IA, Lankreijer H, Matteucci G *et al*. (2001) Productivity overshadows temperature in determining soil and ecosystem respiration across European forests. *Global Change Biology*, **7**, 269–278.

Kindermann J, Wurth G, Kohlmaier GH, Badeck FW (1996) Interannual variation of carbon exchange fluxes in terrestrial ecosystems. *Global Biogeochemical Cycles*, **10**, 737–755.

Kiviluoto K (1996) Topology preservation in self-organizing maps. In: *Proceedings of the International Conference on Neural Networks (ICNN'96)*, Vol. 1 (ed. CINN), pp. 294–299. Piscataway, New Jersey.

Kljun N, Black TA, Griffis TJ, Barr AG, Gaumont-Guay D, Morgenstern K, McCaughey JH, Nesic Z (2006) Response of net ecosystem productivity of three boreal forest stands to drought. *Ecosystems*, **9**, 1128–1144.

Kohonen T (2001) *Self-Organizing Maps*. Springer-Verlag, Berlin.

Launiainen S, Rinne J, Pumpanen J *et al*. (2005) Eddy covariance measurements of CO_2 and sensible and latent heat fluxes during a full year in a boreal pine forest trunk-space. *Boreal Environment Research*, **10**, 569–588.

Law BE, Falge E, Gu L *et al*. (2002) Environmental controls over carbon dioxide and water vapor exchange of terrestrial vegetation. *Agricultural and Forest Meteorology*, **113**, 97–120.

Loescher HW, Law BE, Mahrt L, Hollinger DY, Campbell J, Wofsy SC (2006) Uncertainties in, and interpretation of, carbon flux estimates using the eddy covariance technique. *Journal of Geophysical Research-Atmospheres*, **111**, D21S90, doi: 10.1029/2005JD006932.

Meehl GA, Tebaldi C (2004) More intense, more frequent, and longer lasting heat waves in the 21st century. *Science*, **305**, 994–997.

Moffat AM, Papale D, Reichstein M *et al*. (2007) Comprehensive comparison of gap filling techniques for eddy covariance net carbon fluxes. *Agricultural and Forest Meteorology*, doi: 10.1016/j.agrformet.2007.08.011.

Monson RK, Turnipseed AA, Sparks JP, Harley PC, Scott-Denton LE, Sparks K, Huxman TE (2002) Carbon sequestration in a high-elevation, subalpine forest. *Global Change Biology*, **8**, 459–478.

Oja M, Kaski S, Kohonen T (2003) Bibliography of self-organizing map (SOM) papers: 1998–2001 addendum. *Neural Computing Surveys*, **3**, 1–156.

Papale D, Reichstein M, Aubinet M *et al*. (2006) Towards a standardized processing of net ecosystem exchange measured with eddy covariance technique: algorithms and uncertainty estimation. *Biogeosciences*, **3**, 571–583.

Papale D, Valentini A (2003) A new assessment of European forests carbon exchanges by eddy fluxes and artificial neural network spatialization. *Global Change Biology*, **9**, 525–535.

Randerson JT, Field CB, Fung IY, Tans PP (1999) Increases in early season ecosystem uptake explain recent changes in the seasonal cycle of atmospheric CO_2 at high northern latitudes. *Geophysical Research Letters*, **26**, 2765–2768.

Reichstein M, Falge E, Baldocchi D *et al*. (2005) On the separation of net ecosystem exchange into assimilation and ecosystem respiration: review and improved algorithm. *Global Change Biology*, **11**, 1424–1439.

Reichstein M, Papale D, Valentini R *et al*. (2007) Determinants of terrestrial ecosystem carbon balance inferred from European eddy covariance flux sites. *Geophysical Research Letters*, **34**, L01402, doi: 10.1029/2006GL027880.

Richardson AD, Hollinger DY, Burba GG *et al*. (2006) A multi-site analysis of random error in tower-based measurements of carbon and energy fluxes. *Agricultural and Forest Meteorology*, **136**, 1–18.

Ryan MG, Law BE (2005) Interpreting, measuring, and modeling soil respiration. *Biogeochemistry*, **73**, 3–27.

Sagarin R (2001) False estimates of the advance of spring. *Nature*, **414**, 600.

Schär C, Vidale PL, Lüthi D, Frei C, Häberli C, Liniger MA, Appenzeller C (2004) The role of increasing temperature variability in European summer heatwaves. *Nature*, **427**, 332–336.

Schwarz PA, Law BE, Williams M, Irvine J, Kurpius M, Moore D (2004) Climatic versus biotic constraints on carbon and water fluxes in seasonally drought-affected ponderosa pine ecosystems. *Global Biogeochemical Cycles*, **18**, GB4007, doi: 10.1029/2004GB002234.

Stoy PC, Katul GG, Siqueira MBS, Juang JY, McCarthy HR, Kim HS, Oishi AC, Oren R (2005) Variability in net ecosystem exchange from hourly to inter-annual time scales at adjacent pine and hardwood forests: a wavelet analysis. *Tree Physiology*, **25**, 887–902.

Suni T, Berninger F, Markkanen T, Keronen P, Rannik Ü, Vesala T (2003a) Interannual variability and timing of growing-season CO_2 exchange in a boreal forest. *Journal of Geophysical Research-Atmospheres*, **108**, 4265–4273.

Suni T, Berninger F, Vesala T *et al*. (2003b) Air temperature triggers the recovery of evergreen boreal forest photosynthesis in spring. *Global Change Biology*, **9**, 1410–1426.

Tang JW, Baldocchi DD, Xu L (2005) Tree photosynthesis modulates soil respiration on a diurnal time scale. *Global Change Biology*, **11**, 1298–1304.

Tian HQ, Melillo JM, Kicklighter DW, McGuire AD, Helfrich JVK, Moore B, Vorosmarty CJ (1998) Effect of interannual climate variability on carbon storage in Amazonian ecosystems. *Nature*, **396**, 664–667.

© 2007 The Authors

Valentini R, Matteucci G, Dolman AJ *et al*. (2000) Respiration as the main determinant of carbon balance in European forests. *Nature*, **404**, 861–865.

van der Werf GR, Randerson JT, Collatz GJ, Giglio L, Kasibhatla P, Arellano AF, Olsen SC, Kasischke ES (2004) Continental-scale partitioning of fire emissions during the 1997 to 2001 El Nino period. *Science*, **303**, 73–76.

van Dijk AIJM, Dolman AJ, Schulze ED (2005) Radiation, temperature, and leaf area explain ecosystem carbon fluxes in boreal and temperate European forests. *Global Biogeochemical Cycles*, **19**, GB2029, doi: 10.1029/2004GB002417.

Vesala T, Suni T, Rannik Ü *et al*. (2005) Effect of thinning on surface fluxes in a boreal forest. *Global Biogeochemical Cycles*, **19**, GB2001, doi: 10.1029/2004GB002316.

Appendix A: Self-Organizing Map (SOM)

The SOM consists of a regular, usually a two-dimensional, grid of neurons. The neurons are connected to adjacent neurons by a neighborhood function. Each neuron on the two-dimensional grid also has a d-dimensional prototype vector $\mathbf{m}$, where d is the dimension of the data vectors $\mathbf{x}$. In this study $\mathbf{x} = [\delta_{NEE}, \delta_{GPP}, \delta_{Re}, T_a, R_g, VPD_{max}, P_r$, Bowen], where δ denotes an anomaly. Thus, SOM defines a nonlinear projection from the d-dimensional data space to the two-dimensional grid. Conceptually, SOM and its neurons form an elastic net in the data space. During training the SOM is trained to represent the original data by adapting its prototype vectors according to the dataset. Thus, in addition to nonlinear projection, SOM also performs vector quantization. This representation can be used for visualization, clustering and exploration of the data (Kohonen, 2001).

The mapping from the original data space to the grid of neurons tends to preserve topological relationships. This means that the data vectors close to each other in the data space tend to map to the same or close-by neurons in the grid (in the sense of the neighborhood function). This makes visualization of the grid useful in exploring the relationships of variables and the possible cluster structure of the data. Without the neighborhood function the SOM algorithm reduces to the k-means algorithm (Kohonen, 2001).

Before training, the number of neurons and the structure of the grid in the SOM are defined. The dimension of the grid is determined by the dimension of the dataset. After initializing the neurons with values spanning the space of two dominant eigenvectors, the training proceeds in two alternating steps: the data vectors are first mapped to neurons by looking for the best-matching unit (or the neuron with the closest prototype vector) using a Euclidean distance measure between the data vector and the set of neurons. Second, the neurons are adapted to better represent the distribution of the data. Usually, the training is done in two phases: a coarse training is followed by a fine-tuning of the neurons.

The data vectors $\mathbf{x}$ have to be normalized before training such that the mean of each variable is 0 and the variance is 1. The normalization method scales the data linearly, which preserves the structure of the absolute values of the measurements. The method used to normalize the data defines the distance between multidimensional vectors. For example, how should a change of 1 °C in air temperature be related to a change of 1.0 kPa in vapor pressure? Normalizing all the variances to unity solves this problem by defining that changes in different variables are equal if they are in equal proportion to their standard deviations. As a result, all variables have equal weights. Therefore it is not desirable to use different measures of the same process, i.e. global and net radiation or air and soil temperature in the same SOM. When for example air and soil temperature are used to train the SOM, the effect of temperature will be overestimated by the SOM. Normalizing the data is technically convenient, but it has serious drawbacks in biological terms if the data processing methods seek an explanation of the variance, as in principal component analysis and other methods. However, the SOM applied in this study is not used to explain the variance of the data. As further data processing and interpretation are based on the observed data, normalization does not have any drawbacks.

The fit of the model can be measured with the quantization error, which is the average distance from each data vector to its best-matching unit. The value of the error is given in normalized units, i.e. a value of 1 means that the average (in our case eight-dimensional) distance equals the standard deviation of a single variable. The average quantization error was 0.66, 0.89 and 0.93 for Hyytiälä, Loobos and Le Bray, respectively (for a randomly generated normal distributed dataset the quantization error was 1.76). The quantization error can be decreased by increasing the number of neurons, but this has the drawback, that the number of data vectors per neuron decreases, which may lead to overfitting. In addition to quantization, the topology preservation of the projection can be measured with the topographic error (Kiviluoto, 1996). This is defined as the percentage of data vectors for which the best-matching unit and the second-best-matching unit are not neighboring units on the grid. The topological error was 6% for Hyytiälä and 9% for Loobos and Le Bray. Owing to the low number of topographic errors, the topology of the dataset was thus preserved well in the quantization process. Therefore, the SOM was expected to give reliable results.

© 2007 The Authors